ELSEVIER

Journal of Fluids and Structures 24 (2008) 732–749

JOURNAL OF FLUIDS AND STRUCTURES

www.elsevier.com/locate/jfs

# Convergence predictions for aeroelastic calculations of tuned and mistuned bladed disks ☆

Z. He[a], B.I. Epureanu[a,*], C. Pierre[b]

[a]*Department of Mechanical Engineering, University of Michigan, 2350 Hayward Street, Ann Arbor, MI 48109-2125, USA*
[b]*Faculty of Engineering, McGill University, 817 Sherbrooke Street, Montreal, Que., Canada H3A-2K6*

Received 6 April 2006; accepted 29 October 2007
Available online 5 March 2008

**Abstract**

Mistuning changes the dynamics of bladed disks significantly. Frequency domain methods for predicting the dynamics of mistuned bladed disks are typically based on iterative aeroelastic calculations. Converged aerodynamic stiffness matrices are required for accurate aeroelastic results of eigenvalue and forced response problems. The tremendous computation time needed for each aerodynamic iteration would greatly benefit from a fast method of predicting the number of iterations needed for converged results. A new hybrid technique is proposed to predict the convergence history based on several critical ratios and by approximating as linear the relation between the aerodynamic force and the complex frequencies (eigenvalues) of the system. The new technique is hybrid in that it uses a combined theoretical and stochastic/computational approach. The dynamics of an industrial bladed disk is investigated, and the predicted convergence histories are shown to match the actual results very well. Monte Carlo simulations using the new hybrid technique show that the aerodynamic ratio and the aerodynamic gradient ratio are the two most important factors affecting the convergence history.


*Keywords:* Aeroelasticity; Turbomachinery; Bladed disks; Iterative methods; CFD

## 1. Introduction

Mistuning, small differences between the sectors of bladed disks, can lead to drastic changes in the dynamics of such systems. The large increase in the forced response of the system due to mistuning has been observed and studied for a long time (Anderson, 1958; Tobias and Arnold, 1957).

Recently, compact and accurate reduced order models (ROMs) have been developed (Bladh et al., 2001a, b; Lim et al., 2003; Yang and Griffin, 2001a, b; Feiner and Griffin, 2002; Petrov et al., 2002). In particular, the fundamental mistuning model (FMM) (Feiner and Griffin, 2002) and the component mode mistuning (CMM) (Lim et al., 2003) method have been proposed. These approaches use one group of tuned system modes as basis for model reduction. The results obtained without aerodynamic coupling and by using these ROMs have been shown to be as accurate as the results obtained using the finite element method (FEM) (Lim et al., 2003; Feiner and Griffin, 2002). However,

☆An earlier version of this work has been presented at the 2006 ASME PVP Conference, Vancouver, Canada.

*Corresponding author.
*E-mail address:* epureanu@umich.edu (B.I. Epureanu).

0889-9746/$ - see front matter © 2007 Elsevier Ltd. All rights reserved.
doi:10.1016/j.jfluidstructs.2007.10.014

realistic bladed disks are coupled not only structurally, but also aerodynamically. Previous studies on lumped structural parameter models showed that interblade structural coupling and mistuning are two key factors affecting mistuned systems (Wei and Pierre, 1988a, b). Aerodynamic forces, which provide aerodynamic damping as well as blade-to-blade coupling, may change the dynamics of the system dramatically. Also, the flutter problem arises when aerodynamic forces are considered. Hence, the inclusion of aerodynamic coupling in current ROMs is necessary.

Early studies on the frequency domain aeroelastic problem of mistuned bladed disks used simple structural and aerodynamic models (Kaza and Kielb, 1984, 1985; Crawley and Hall, 1985; Khader and Loewy, 1989). In these simple models, the blades are usually represented by two-dimensional airfoils or cantilevered beams, and they can only have rigid body mode shapes, e.g. pitch and plunge motions, which are far from the real three-dimensional elastic motion. Recently, the aerodynamic calculation of unsteady pressure induced by elastic blade motions has been studied intensely, and numerous models have been proposed (Hall, 1993; Hall and Lorence, 1993; Chaviaropoulos and Hansen, 2000; Fransson et al., 1999; Bell and He, 2000). However, the applications of these aerodynamic models to aeroelastic calculations are limited. Kielb et al. (2004a, b) incorporated a three-dimensional Reynolds averaged Navier–Stokes (RANS) CFD code into the FMM model (Feiner and Griffin, 2002). He et al. (2005a) incorporated a quasi-three-dimensional potential flow CFD code into the CMM model (Lim et al., 2003). Both methods use the cantilever-blade normal modes (in the complex traveling wave coordinates) and their vibration frequencies to calculate the unsteady aerodynamic forces. Seinturier et al. (2002) used both cantilevered blade modes and constraint modes to calculate the unsteady aerodynamic forces.

Few studies have been conducted on the *true*, *realistic* aeroelastic calculations. Gerolymos (1993) used a mode-modification technique to solve the tuned aeroelastic eigenvalue problem. Moyroud et al. (1996) proposed a direct iterative method to calculate the aeroelastic eigenvalue problem. He et al. (2005b) used the tuned structural system modes and the aeroelastic frequencies to calculate the aerodynamic forces with an iterative method. These studies have shown that the converged tuned and mistuned results have significant differences compared to the one-step results or the results using the blade normal modes.

In He et al. (2005b), the aeroelastic calculation requires much less computational time for the tuned case compared to the mistuned case. The tuned cases require about 0.5 h for one step on a SunBlade-1000 machine and up to five steps to converge. The mistuned cases require about 10 h for one step, and usually require more steps to converge compared to the tuned cases. Such large amounts of computation time make it very important to be able to predict the number of iterations needed to get converged results. This paper proposes a new hybrid method to predict the convergence history. Several critical ratios are introduced to represent the properties of the system. This new technique is hybrid in that it uses both exact information from accurate models as well as randomly generated Monte Carlo models which allow for stochastic predictions for general aeroelastic configurations (He et al., 2006). The relation between the unsteady aerodynamic forces and the aeroelastic frequencies is approximated by a linear relation, which holds for many cases. For example, in many aeroelastic problems, the changes in frequency during the iterative process are small because structural stiffness dominates the aerodynamic stiffness. Hence, structural frequencies are good starting states for the iterative calculations (initial guesses). Also, good initial guesses may be available from previous calculations, as is the case for design optimization applications. Herein, the new hybrid technique is applied to a realistic bladed disk. The simulated convergence histories give good predictions for the actual convergence histories. Monte Carlo simulations using the new hybrid technique with varying critical ratios show that the magnitudes of aerodynamic matrices and their gradients with respect to the aeroelastic frequencies are two key factors affecting the convergence history.

## 2. Aeroelastic model

This section summarizes the approach used to include aerodynamic effects within the CMM method by using the tuned structure-only system modes with iterations over natural frequencies and mode shapes. For a complete description of the aeroelastic models using the cantilever-blade normal modes and the tuned structure-only system modes, one may refer to He et al. (2005a, b). Note that the tuned aeroelastic calculation is not discussed separately here because it is similar to the mistuned aeroelastic calculation.

In the tuned system modal space (employed by FMM and CMM methods), the modal equations for the eigenvalue and forced response problems can be expressed as (Lim et al., 2003; He et al., 2005b)

$$[(1+\mathrm{j}\gamma)\mathbf{K}^{\mathrm{syn}}+\mathbf{K}^{a}-\omega^{2}\mathbf{M}^{\mathrm{syn}}]\mathbf{q}_{\phi}^{S}=\mathbf{0} \tag{1}$$

and

$$[(1+\mathrm{j}\gamma)\mathbf{K}^{\mathrm{syn}}+\mathbf{K}^{a}-\omega^{2}\mathbf{M}^{\mathrm{syn}}]\mathbf{q}_{\phi}^{S}=\mathbf{\Phi}_{\Gamma}^{S,0*}\mathbf{f}, \tag{2}$$

where the asterisk denotes the Hermitian of a complex matrix, $\mathrm{j}=\sqrt{-1}$, $\mathbf{\Phi}^{S,0}$ is a truncated set of normal modes (in the frequency range of interest) of the tuned system with structural coupling only, subscript $\Gamma$ denotes the blade DOFs, $\mathbf{q}_{\phi}^{S}$ are the corresponding modal coordinates, $\mathbf{K}^{a}$ is the complex aerodynamic coupling (stiffness) matrix related to $\mathbf{\Phi}^{S,0}$, $\gamma$ is the modal structural damping, $\mathbf{f}$ is the physical force acting on the blades, and the matrices $\mathbf{M}^{\mathrm{syn}}$ and $\mathbf{K}^{\mathrm{syn}}$ are the whole modal mass and stiffness matrices, including the structural stiffness and mass mistuning components. Note that only structural stiffness mistuning is considered in this paper, and the tuned structure-only system modes $\mathbf{\Phi}^{S,0}$ are normalized with respect to the tuned mass matrix in the physical domain. Hence, $\mathbf{M}^{\mathrm{syn}}=\mathbf{I}$. Also, note that $\mathbf{K}^{a}\mathbf{q}_{\phi}^{S}$ represents the modal aerodynamic forces. Therefore, linearity between the blade motion and the aerodynamic forces induced by the blade motion is assumed. Such linearity holds when the blade motions are small (Hall, 1993; Hall and Lorence, 1993). However, the dependence of the aerodynamic forces on the complex vibration frequency is nonlinear (Hall, 1993), which requires iterative calculations for accurate aeroelastic results. Note that $\mathbf{K}^{a}$ is a complex matrix.

Due to cyclic symmetry, the tuned structure-only modes can be expressed in a standing wave form or a traveling wave form (Bladh, 2001). In this paper, the traveling wave form is used. Hence, for every tuned structure-only mode, a constant phase angle $\sigma_i$ between adjacent sectors exists, which is referred to as the interblade phase angle

$$\sigma_i=\frac{2\pi i}{N_B},\quad i=0,1,\ldots,N_B-1, \tag{3}$$

where $N_B$ is the number of blades, and $i$ is the traveling wave index associated with the tuned system mode. For $i=0$ and $i=N_B/2$ (if $N_B$ is even), the traveling wave and the standing wave are the same. For $i=1$ to $i=(N_B-2)/2$ (if $N_B$ is even) or $i=(N_B-1)/2$ (if $N_B$ is odd), $\sigma_i$ and $\sigma_{N_B-i}$ correspond to the same nodal diameter $i$, but with opposite traveling directions. The undamped tuned structure-only system modes related to $\sigma_i$ and $\sigma_{N_B-i}$ are complex conjugates. Their real and imaginary parts are the corresponding standing wave modes. It is easy to show that traveling waves with different interblade phase angles are orthogonal to each other (Bladh, 2001).

The aeroelastic system modes can be obtained from Eq. (1) as

$$\mathbf{\Phi}_{\Gamma,i}^{S,n}=\sum_{r=1}^{N_S}Q_{\phi,ri}^{S,n}\mathbf{\Phi}_{\Gamma,r}^{S,0},\quad i=1,2,\ldots,N_S, \tag{4}$$

or in matrix form as

$$\mathbf{\Phi}_{\Gamma}^{S,n}=\mathbf{\Phi}_{\Gamma}^{S,0}\mathbf{Q}_{\phi}^{S,n}, \tag{5}$$

where the superscript $n$ denotes results after $n$ steps of iterative calculations, $N_S$ is the number of tuned structure-only system modes used in Eq. (1), and the matrix $\mathbf{Q}_{\phi}^{S,n}$ is in the form of

$$\mathbf{Q}_{\phi}^{S,n}=[\mathbf{q}_{\phi,1}^{S,n}\ \ \mathbf{q}_{\phi,2}^{S,n}\cdots\mathbf{q}_{\phi,N_S}^{S,n}]. \tag{6}$$

The unsteady aerodynamic forces (acting on a blade and) induced by the $i$th aeroelastic system mode $\mathbf{\Phi}_{\Gamma,i}^{S,n}$ can be obtained (using superposition) by the following linear relation:

$$\mathbf{F}_{i}^{S,n}=\sum_{r=1}^{N_S}Q_{\phi,ri}^{S,n}\mathbf{F}_{i,r}^{S,0},\quad i=1,2,\ldots,N_S, \tag{7}$$

where $\mathbf{F}_{i}^{S,n}$ is the unsteady aerodynamic force induced by the mode shape $\mathbf{\Phi}_{\Gamma,i}^{S,n}$, and $\mathbf{F}_{i,r}^{S,0}$ is the unsteady aerodynamic force induced by the $r$th tuned structure-only system mode shape $\mathbf{\Phi}_{\Gamma,r}^{S,0}$. Note that, at the $n$th iteration step, the mode $\mathbf{\Phi}_{i,r}^{S,0}$ vibrates with the $i$th *mistuned* complex system natural frequency $\omega_i^n$ (where $\omega_i^n$ is complex; see Eq. (1)). Hence, $\mathbf{F}_{i,r}^{S,0}$ is also related to $\omega_i^n$. The elements of the aerodynamic matrix (in the mistuned aeroelastic system modal coordinates) $\hat{\mathbf{A}}^{M,n}$ can be expressed as

$$\hat{\mathbf{A}}_{ij}^{M,n}=\mathbf{\Phi}_{\Gamma,i}^{S,n*}\mathbf{F}_{j}^{S,n}=\left(\sum_{r=1}^{N_S}Q_{\phi,ri}^{S,n\,*}\mathbf{\Phi}_{\Gamma,r}^{S,0*}\right)\left(\sum_{t=1}^{N_S}Q_{\phi,tj}^{S,n}\mathbf{F}_{j,t}^{S,0}\right)=\sum_{r=1}^{N_S}\sum_{t=1}^{N_S}Q_{\phi,ri}^{S,n\,*}\mathbf{\Phi}_{\Gamma,r}^{S,0*}Q_{\phi,tj}^{S,n}\mathbf{F}_{j,t}^{S,0}. \tag{8}$$

The calculations in Eq. (8) can be simplified using the orthogonality between $\mathbf{\Phi}_{\Gamma,r}^{S,0}$ and $\mathbf{F}_{j,t}^{S,0}$ with different interblade phase angles. The aerodynamic matrix in the tuned structure-only system modal coordinates can be derived by using the

modal transformation shown in Eq. (5). One obtains

$$\mathbf{K}^{a,n} = \mathbf{P}^{n*}\hat{\mathbf{A}}^{M,n}\mathbf{P}^{n}, \tag{9}$$

where $\mathbf{P}^{n} = (\mathbf{Q}_{\phi}^{S,n})^{-1}$ is the modal transformation from the mistuned aeroelastic system modes to the tuned structure-only system modes.

After each iteration $n$, the matrix $\mathbf{K}^{a,n}$ is compared to $\mathbf{K}^{a,n-1}$ and the iterative process continues until their values are converged. An aerodynamic matrix with zero elements is used for the first step of iteration.

## 3. Hybrid technique: general case

In this section, for clarity, $\mathbf{F}(\omega_i^n, \mathbf{\Phi}_{\Gamma,r}^{S,n})$ is used to replace $\mathbf{F}_i^{S,n}$ and $\mathbf{F}(\omega_i^n, \mathbf{\Phi}_{\Gamma,r}^{S,0})$ is used to replace $\mathbf{F}_{i,r}^{S,0}$ in Eq. (7). Hence, Eq. (7) can be rewritten as

$$\mathbf{F}(\omega_i^n, \mathbf{\Phi}_{\Gamma,r}^{S,n}) = \sum_{r=1}^{N_S} Q_{\phi,ri}^{S,n}\mathbf{F}(\omega_i^n, \mathbf{\Phi}_{\Gamma,r}^{S,0}), \quad i = 1,2,\ldots,N_S. \tag{10}$$

From Eqs. (5), (8), and (9), $\mathbf{K}^{a,n}$ can be expressed as

$$\mathbf{K}^{a,n} = \mathbf{P}^{n*}\hat{\mathbf{A}}^{M,n}\mathbf{P}^{n} = \mathbf{P}^{n*}\mathbf{Q}_{\phi}^{S,n*}\hat{\mathbf{A}}_0^{M,n}\mathbf{P}^{n} = \hat{\mathbf{A}}_0^{M,n}\mathbf{P}^{n}, \tag{11}$$

where the elements of matrix $\hat{\mathbf{A}}_0^{M,n}$ can be obtained using Eq. (10) as follows:

$$\hat{\mathbf{A}}_{0,ij}^{M,n} = \mathbf{\Phi}_{\Gamma,i}^{S,0*}\mathbf{F}(\omega_j^n, \mathbf{\Phi}_{\Gamma,r}^{S,n}) = \sum_{r=1}^{N_S} Q_{\phi,rj}^{S,n}\mathbf{\Phi}_{\Gamma,i}^{S,0*}\mathbf{F}(\omega_j^n, \mathbf{\Phi}_{\Gamma,r}^{S,0}). \tag{12}$$

Usually, the aerodynamic calculation to obtain each term $\mathbf{\Phi}_{\Gamma,i}^{S,0*}\mathbf{F}(\omega_j^n, \mathbf{\Phi}_{\Gamma,r}^{S,0})$ in Eq. (12) is very time consuming because of the large dimension of the overall problem as well as the eigenvalue analysis required for the far field nonreflective boundary conditions (Hall et al., 1993). Hence, parametric studies for the convergence history are formidably expensive computationally. To overcome this difficulty, changes in aerodynamic forces $\mathbf{F}(\omega_j^n, \mathbf{\Phi}_{\Gamma,r}^{S,0})$ due to changes in aeroelastic frequencies are approximated by assuming a linear dependence of aerodynamic forces on vibration frequencies. Fig. 2 shows a typical variation of the natural frequency $\omega_{R,j}^0$ (i.e. real part of $\omega_j^0$) as a function of nodal diameter diagram, where each nodal diameter represents an interblade phase angle of a tuned system mode. The horizontal lines correspond to blade dominant modes, while the slant lines correspond to disk dominant modes. Usually, the frequency range covering only one group of blade dominant system modes is considered, so the differences between the aeroelastic frequencies are small. Although the actual dependence of aerodynamic forces on the frequencies is nonlinear, their linear approximation can give reasonable predictions about the convergence history. Also, the real and imaginary parts of the complex aeroelastic frequency are assumed to be two independent variables because the gradient of the aerodynamic forces with respect to these two variables can be distinct. Under this assumption, $\mathbf{F}(\omega_j^n, \mathbf{\Phi}_{\Gamma,r}^{S,0})$ can be expressed as

$$\mathbf{F}(\omega_j^n, \mathbf{\Phi}_{\Gamma,r}^{S,0}) \approx \mathbf{F}(\omega_r^0, \mathbf{\Phi}_{\Gamma,r}^{S,0}) + \mathbf{D}_R(\omega_r^0, \mathbf{\Phi}_{\Gamma,r}^{S,0})\frac{\omega_{R,j}^n - \omega_{R,r}^0}{\omega_{\text{ref}}} + \mathbf{D}_I(\omega_r^0, \mathbf{\Phi}_{\Gamma,r}^{S,0})\frac{\omega_{I,j}^n - \omega_{I,r}^0}{\omega_{\text{ref}}}, \tag{13}$$

where a subscript $R$ denotes the real part of the complex frequency, and a subscript $I$ denotes the imaginary part of the complex frequency, $\mathbf{D}(\omega_r^0, \mathbf{\Phi}_{\Gamma,r}^{S,0})$ is the linear coefficient of the aerodynamic force to the relative changes of natural frequencies, $\omega_r^0$ is the $r$th structure-only complex frequency, and $\omega_{\text{ref}}$ is a reference frequency. Because only one group of blade dominant modes is considered, the mean value of the corresponding frequencies for these modes is used as $\omega_{\text{ref}}$ in this paper, except in the case of a tuned case, as discussed in Section 4. Note that the unit for $\omega$ is rad/s instead of Hz here. Therefore, one can rewrite Eq. (12) as

$$\hat{\mathbf{A}}_{0,ij}^{M,n} \approx \sum_{r=1}^{N_S} Q_{\phi,rj}^{S,n}\mathbf{\Phi}_{\Gamma,i}^{S,0*}\left[\mathbf{F}(\omega_r^0, \mathbf{\Phi}_{\Gamma,r}^{S,0}) + \mathbf{D}_R(\omega_r^0, \mathbf{\Phi}_{\Gamma,r}^{S,0})\frac{\omega_{R,j}^n - \omega_{R,r}^0}{\omega_{\text{ref}}} + \mathbf{D}_I(\omega_r^0, \mathbf{\Phi}_{\Gamma,r}^{S,0})\frac{\omega_{I,j}^n - \omega_{I,r}^0}{\omega_{\text{ref}}}\right], \tag{14}$$

or

$$\hat{\mathbf{A}}_{0,ij}^{M,n} \approx \sum_{r=1}^{N_S}\left[\boldsymbol{\Phi}_{\Gamma,i}^{S,0*}\mathbf{F}(\omega_r^0,\boldsymbol{\Phi}_{\Gamma,r}^{S,0})Q_{\phi,rj}^{S,n} + \boldsymbol{\Phi}_{\Gamma,i}^{S,0*}\mathbf{D}_R(\omega_r^0,\boldsymbol{\Phi}_{\Gamma,r}^{S,0})\left(Q_{\phi,rj}^{S,n}\frac{\omega_{R,j}^n-\omega_{R,r}^0}{\omega_{\mathrm{ref}}}\right)\right.$$
$$\left. + \boldsymbol{\Phi}_{\Gamma,i}^{S,0*}\mathbf{D}_I(\omega_r^0,\boldsymbol{\Phi}_{\Gamma,r}^{S,0})\left(Q_{\phi,rj}^{S,n}\frac{\omega_{I,j}^n-\omega_{I,r}^0}{\omega_{\mathrm{ref}}}\right)\right]. \tag{15}$$

By examining Eq. (15), five matrices are defined as

$$\mathbf{A}_{0,ij} = \boldsymbol{\Phi}_{\Gamma,i}^{S,0*}\mathbf{F}(\omega_j^0,\boldsymbol{\Phi}_{\Gamma,j}^{S,0}),\quad \mathbf{G}_{0,ij}^R = \boldsymbol{\Phi}_{\Gamma,i}^{S,0*}\mathbf{D}_R(\omega_j^0,\boldsymbol{\Phi}_{\Gamma,j}^{S,0}),\quad \mathbf{G}_{0,ij}^I = \boldsymbol{\Phi}_{\Gamma,i}^{S,0*}\mathbf{D}_I(\omega_j^0,\boldsymbol{\Phi}_{\Gamma,j}^{S,0}), \tag{16,17,18}$$

$$\mathbf{T}_{R,ij}^n = Q_{\phi,ij}^{S,n}\frac{\omega_{R,j}^n-\omega_{R,i}^0}{\omega_{\mathrm{ref}}},\quad \mathbf{T}_{I,ij}^n = Q_{\phi,ij}^{S,n}\frac{\omega_{I,j}^n-\omega_{I,i}^0}{\omega_{\mathrm{ref}}}. \tag{19,20}$$

Hence, Eq. (15) can be rewritten in a matrix form

$$\hat{\mathbf{A}}_0^{M,n} = \mathbf{A}_0\mathbf{Q}_\phi^{S,n} + \mathbf{G}_0^R\mathbf{T}_R^n + \mathbf{G}_0^I\mathbf{T}_I^n. \tag{21}$$

Finally, the aerodynamic matrix in the tuned structure-only system modal space $\mathbf{K}^{a,n}$ can be obtained as

$$\mathbf{K}^{a,n} = \mathbf{A}_0 + \mathbf{G}_0^R\mathbf{T}_R^n\mathbf{P}^n + \mathbf{G}_0^I\mathbf{T}_I^n\mathbf{P}^n. \tag{22}$$

The linear dependence of $\mathbf{K}^{a,n}$ on $\mathbf{T}_R^n$ and $\mathbf{T}_I^n$ reflects the linear approximation in Eq. (13). Due to the orthogonality of vectors with different interblade phase angles, $\mathbf{A}_0$ and $\mathbf{G}_0$ are block diagonal matrices in which every block corresponds to one interblade phase angle. Moreover, $\mathbf{A}_0$ is precisely the tuned aerodynamic matrix after the first step in the iterative calculation. In fact, during the first-step calculation, an aerodynamic matrix with zero entries is used. Hence, the aeroelastic eigenvalues and eigenvectors are the structure-only ones. Thus, both $\mathbf{P}^n$ and $\mathbf{Q}_\phi^{S,n}$ are identity matrices, and $\omega_j^n-\omega_i^0=0$ when $j=i$. This results in $\mathbf{T}_R^n=\mathbf{0}$, $\mathbf{T}_I^n=\mathbf{0}$ and $\mathbf{K}^{a,n}=\mathbf{A}_0$; $\mathbf{A}_0$ is referred to as the aerodynamic (coefficient) matrix. $\mathbf{G}_0^R$ and $\mathbf{G}_0^I$ represent ratios between the change of every entry in $\mathbf{A}_0$ and the change of the corresponding complex natural frequency. $\mathbf{G}_0^R$ and $\mathbf{G}_0^I$ are referred to as the frequency gradient matrices and they can be estimated easily by changing the real and imaginary parts of the eigenvalues and recalculating the tuned aerodynamic matrix. $\mathbf{T}_R^n$ and $\mathbf{T}_I^n$ account for the effect of the complex frequency changes into the modal transform matrix between the aeroelastic and structure-only modal spaces. Note that $\mathbf{A}_0$, $\mathbf{G}_0^R$ and $\mathbf{G}_0^I$ are constant during the iterative calculations, which provides very important computational savings.

To investigate the effects of various factors on the iterative process, several ratios are defined as follows:

$$r_A = \frac{\|\mathbf{A}_0\|}{\omega_{\mathrm{ref}}^2},\quad r_G = \frac{\sqrt{\|\mathbf{G}_0^R\|^2+\|\mathbf{G}_0^I\|^2}}{\|\mathbf{A}_0\|}, \tag{23,24}$$

$$r_F = \frac{\sigma(\omega_s^0)}{\omega_{\mathrm{ref}}},\quad r_V = \frac{\omega_D-\omega_B}{\omega_{\mathrm{ref}}},\quad r_M = \frac{\|\mathbf{K}_M^{\mathrm{syn}}\|}{\omega_{\mathrm{ref}}^2}, \tag{25,26,27}$$

where $\|\mathbf{A}_0\|$ denotes the Euclidean norm of $\mathbf{A}_0$, $\sigma(\omega_s^0)$ is the standard deviation of the structural natural frequencies of the blade dominant system modes, $\omega_D$ and $\omega_B$ are the frequencies in the frequency veering region corresponding to the disk and blade dominant modes, and $\mathbf{K}_M^{\mathrm{syn}}$ is the mistuned part of the structural stiffness matrix $\mathbf{K}^{\mathrm{syn}}$. If there is no frequency veering region, $r_V=0$. $r_A$, referred to as the aero ratio, denotes the strength of aerodynamic coupling. $r_G$, referred to as the gradient ratio, denotes the sensitivity of the aerodynamic coupling to natural frequencies. Note that only one gradient ratio is defined, because the magnitudes of $\mathbf{G}_0^R$ and $\mathbf{G}_0^I$ are usually very similar. $r_F$, referred to as the frequency ratio, denotes the spread of the frequencies of the investigated group of blade dominant system modes. $r_F$ is also an indicator of the strength of the structural coupling through the disk. A larger $r_F$ indicates stronger structural coupling. $r_V$, referred to as the veering ratio, denotes the strength of the frequency veering phenomenon. Note, only one frequency veering region is considered in the current study, although multiple frequency veering regions are easy to implement. $r_M$, referred to as the mistuning ratio, denotes the strength of the structural mistuning. The assumption of a linear relationship between the aerodynamic forces and frequency is most likely to be violated when the fluid system is near an instability such as an acoustic resonance or shedding. Predicting the frequency of these fluid instabilities is more complicated, and an alternate method, such as a quadratic approximation may be needed.

## 4. Hybrid technique: tuned case

When a bladed disk is perfectly tuned, no coupling is present between the tuned structure-only system modes with different interblade phase angles. Therefore, a tuned aeroelastic mode can only be a linear combination of the tuned structure-only system modes with the same interblade phase angle. Hence, $\mathbf{Q}_{\phi}^{S,n}$, $\mathbf{P}^n$ and then $\mathbf{T}^n$ are block diagonal matrices, each block corresponding to an interblade phase angle. From Eq. (22), the aerodynamic matrix $\mathbf{K}^{a,n}$ is also a block diagonal matrix. In this case, the whole aeroelastic problem can be decomposed into $N_B$ degraded aeroelastic problems. Therefore, Eqs. (1) and (22) can be simplified as

$$[(1+\mathrm{j}\gamma)\mathbf{\Lambda}_i + \mathbf{K}_i^a - \omega^2\mathbf{I}]\mathbf{q}_{\phi,i}^S = \mathbf{0} \tag{28}$$

and

$$\mathbf{K}_i^{a,n} = \mathbf{A}_{0,i} + \mathbf{G}_{0,i}^R\mathbf{T}_{R,i}^n\mathbf{P}_i^n + \mathbf{G}_{0,i}^I\mathbf{T}_{I,i}^n\mathbf{P}_i^n, \tag{29}$$

where $i = 0, 1, N_B - 1$ is the interblade phase angle index, and $\mathbf{\Lambda}$ is the undamped tuned structural stiffness matrix. The dimension of each aeroelastic problem is the number of tuned structure-only system modes related to the corresponding interblade phase angle $\sigma_i$. Compared to the general case, the dimension of the problem is one order of magnitude smaller. Hence, the computation time saving is very important, especially when parametric studies are desired, such as is the case for the Monte Carlo simulations.

In this paper, only two aeroelastic modes are considered in the simplified tuned case study. Although more aeroelastic modes can be included easily in the computation, in most of practical calculations (like the case of a frequency veering region), it is enough to consider just two modes. For simplicity, the index $i$ is dropped from Eqs. (28) and (29), and a superscript or a subscript $T$ is used to denote the simplified tuned case. For example,

$$\mathbf{\Lambda}_i = \mathbf{\Lambda}^T = \mathrm{Diag}(\omega_{01}^2, \omega_{02}^2), \tag{30}$$

$$\mathbf{K}_i^a = \mathbf{K}_T^a, \quad \mathbf{A}_{0,i} = \mathbf{A}_0^T, \tag{31,32}$$

$$\mathbf{G}_{0,i}^R = \mathbf{G}_0^{TR}, \quad \mathbf{G}_{0,i}^I = \mathbf{G}_0^{TI}, \tag{33,34}$$

where Diag denotes a diagonal matrix, and $\omega_{01}$, $\omega_{02}$ are the two undamped tuned structural frequencies in the veering region. The frequency ratio $r_F$ and mistuning ratio $r_M$ are disregarded in this case, and the veering ratio $r_V^T$ is redefined as

$$r_V^T = \frac{\omega_{02} - \omega_{01}}{\omega_{01}}. \tag{35}$$

## 5. Results and discussion

### 5.1. Case study for an actual bladed disk

In this section, the convergence histories of the aeroelastic calculations for an industrial bladed disk from previous studies (He et al., 2005b) are reproduced using the hybrid technique. The 26-bladed disk shown in Fig. 1 represents a stage of an industrial turbine. Fig. 2 shows the structural natural frequencies versus nodal diameter numbers for the tuned system. Two frequency ranges were studied in (He et al., 2005b). The first one features the first group of system modes (first flexural: 1F), ranging from 500 to 1000 Hz. The other one features the second group of system modes (first torsional: 1T). Because there is a frequency veering region in the 1T frequency range, the dimension for this frequency range is 28. The blade stiffness mistuning pattern considered in this paper has a standard deviation of 0.027 and a mean value of zero. The structural damping used for aeroelastic calculation is 0.001. The mass ratio $\mu$ of the airfoil is 310, where $\mu = m/(\rho\pi b^2)$ with $m$ denoting the mass of the airfoil per unit span, $\rho$ denoting the steady flow density, and $b$ denoting half of the chord length. One step in the iterative calculation consumes about 40 min for the tuned case and 7 h for the mistuned case on a SunBlade-1000 machine. The tuned and mistuned structural modal stiffness matrices can be obtained directly from the CMM computer code *Turbo-Reduce 2002* (Lim et al., 2003). The aerodynamic coefficient matrix $\mathbf{A}_0$ can be obtained after one step of calculation for the tuned system. The frequency gradient matrices $\mathbf{G}_0^R$ and $\mathbf{G}_0^I$ can be calculated as discussed in Section 3. The sensitivity matrices $\mathbf{D}^R$ and $\mathbf{D}^I$ are calculated by using a finite difference approach, i.e., by perturbing the real and imaginary parts of the complex frequency and calculating the

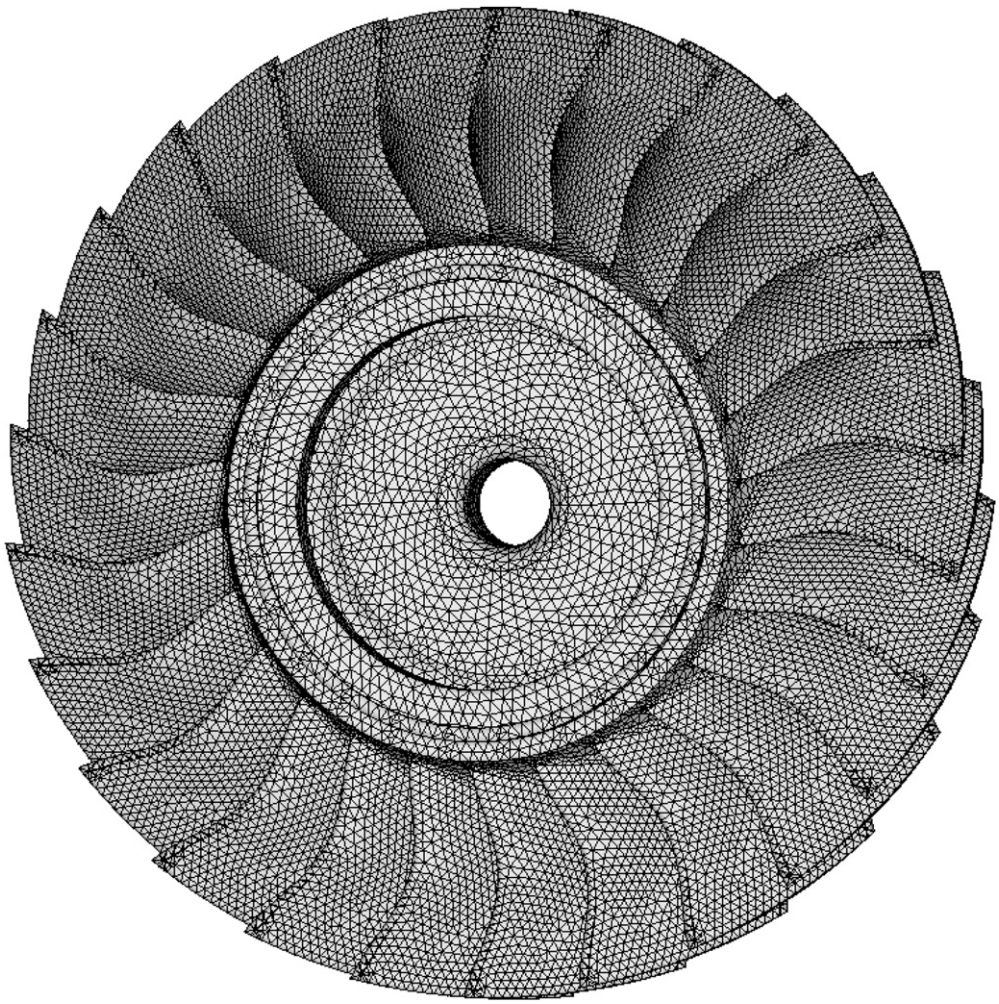

Fig. 1. Finite element model of an industrial bladed disk.

changes in aerodynamic forces. Table 1 shows the reference frequency and the actual ratios for these two frequency ranges. The bladed disk considered here has relatively weak structural coupling and relatively strong aerodynamic damping. For real turbomachinery bladed disks, the frequency variation of structural-only system modes can be as high as 80% for some blisks and the aerodynamic damping is within the range of 1% for most turbomachinery blading. Fig. 3 shows the simulated and actual convergence errors versus number of calculation step for the tuned and mistuned systems in the 1F and 1T frequency ranges. The convergence error is defined as

$$\delta^n = \frac{|\mathbf{K}^a_{n+1} - \mathbf{K}^a_n|}{|\mathbf{K}^a_{n+1}|}, \tag{36}$$

where $|\mathbf{K}^a_n|$ denotes the sum of absolute values of all the entries in the aerodynamic matrix $\mathbf{K}^a$ after $n$th step of calculation. Because $\mathbf{K}^a_0 = \mathbf{0}$ is used, $\delta^0$ is always equal to 1, and hence it is not shown. The actual iteration stops when $\delta^n \leqslant 10^{-5}$. The simulated results match very well the actual results. For the mistuned case, in the 1F frequency range, the differences between the simulated and actual results are slightly larger than those in other cases. These differences are likely caused by the nonlinear relation between the aerodynamic forces and the aeroelastic natural frequencies. Hence, the predictions made for convergence histories are less accurate for cases of strong nonlinear dependence of aerodynamic forces on frequency. Nonetheless, for many cases this dependence is approximately linear. For example, in many aeroelastic problems, the changes in frequency during the iterative process are small because good starting states for the iterative calculations (initial guesses) are available (e.g. from structural frequencies, or from previous calculations, as is the case for design optimization applications). To address general aeroelastic configurations,

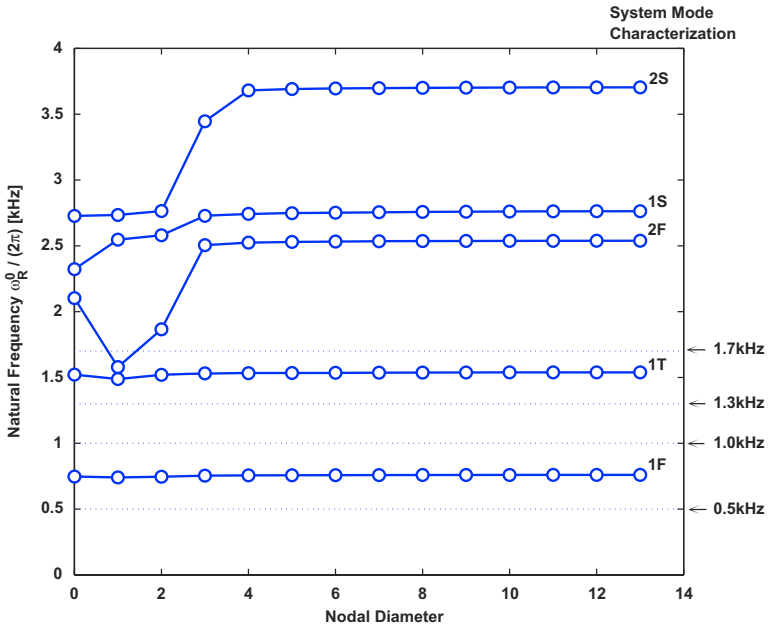


Fig. 2. Natural frequencies versus nodal diameter numbers for the tuned bladed disk assembly.

Table 1
Reference frequency and actual ratios for the 1F and 1T frequency ranges of the industrial bladed disk

| Frequency range | 1F | 1T |
|---|---|---|
| $\omega_{\text{ref}}$ (rad/s) | 4745 | 9616 |
| $r_A$ | 0.237 | 0.289 |
| $r_G$ | 0.625 | 2.415 |
| $r_F$ | $7.96 \times 10^{-3}$ | $8.94 \times 10^{-3}$ |
| $r_V$ | 0.0 | $5.92 \times 10^{-2}$ |
| $r_M$ | 0.131 | 0.0134 |
| $\gamma$ | 0.006 | 0.001 |

perturbed matrices are used. For example, for the matrix $\mathbf{A}_0$, a perturbed matrix $\mathbf{A}_0^P$ is generated by perturbing every entry of $\mathbf{A}_0$ with a random percentage within a certain range. If that certain range is $\varepsilon_A$, an element of $\mathbf{A}_0^P$ can be obtained as

$$\mathbf{A}_{0,ij}^P = (1 + \varepsilon_{A,ij}) \cdot \mathbf{A}_{0,ij}, \quad i,j = 1,2,\ldots,N_S, \tag{37}$$

where $\varepsilon_{A,ij}$ is a random number, and $\varepsilon_{A,ij} \in [-\varepsilon_A, \varepsilon_A]$. Fig. 4 shows the probability density function (PDF) of the convergence errors using the randomly perturbed matrices for the mistuned 1F case. Ten thousand samples are used and the percentage ranges are 0.3 for $\mathbf{A}_0$, $\mathbf{G}_0^R$, and $\mathbf{G}_0^I$, and 0 for others. The actual results are also plotted in Fig. 4. Although the calculation of aerodynamic forces is still linear, the actual results are in the ranges of the PDF or close. Note that, in this case, the numerical simulation requires only about 3 min for each iteration step with 10 000 samples.

Also, one can generate all the matrices randomly using the acquired ratios defined in Section 3. For example, the reference frequency can be set to be the average of the structural frequencies of the blade dominant modes. Next, every entry of $\mathbf{A}_0$ can be generated randomly first, and then the Euclidean norm of $\mathbf{A}_0$ is forced to match the actual aero ratio $r_A$. Fig. 5 shows the PDF of the convergence errors using the totally random matrices for the mistuned 1F case. As shown in Fig. 5, the hybrid technique using totally random numbers with fixed ratios predicts the actual results with good accuracy. One may observe that the ranges of the PDF in Fig. 4 are larger than those in Fig. 5. This is because the sampled space of totally random systems includes the space of slightly perturbed systems. Hence, the actual

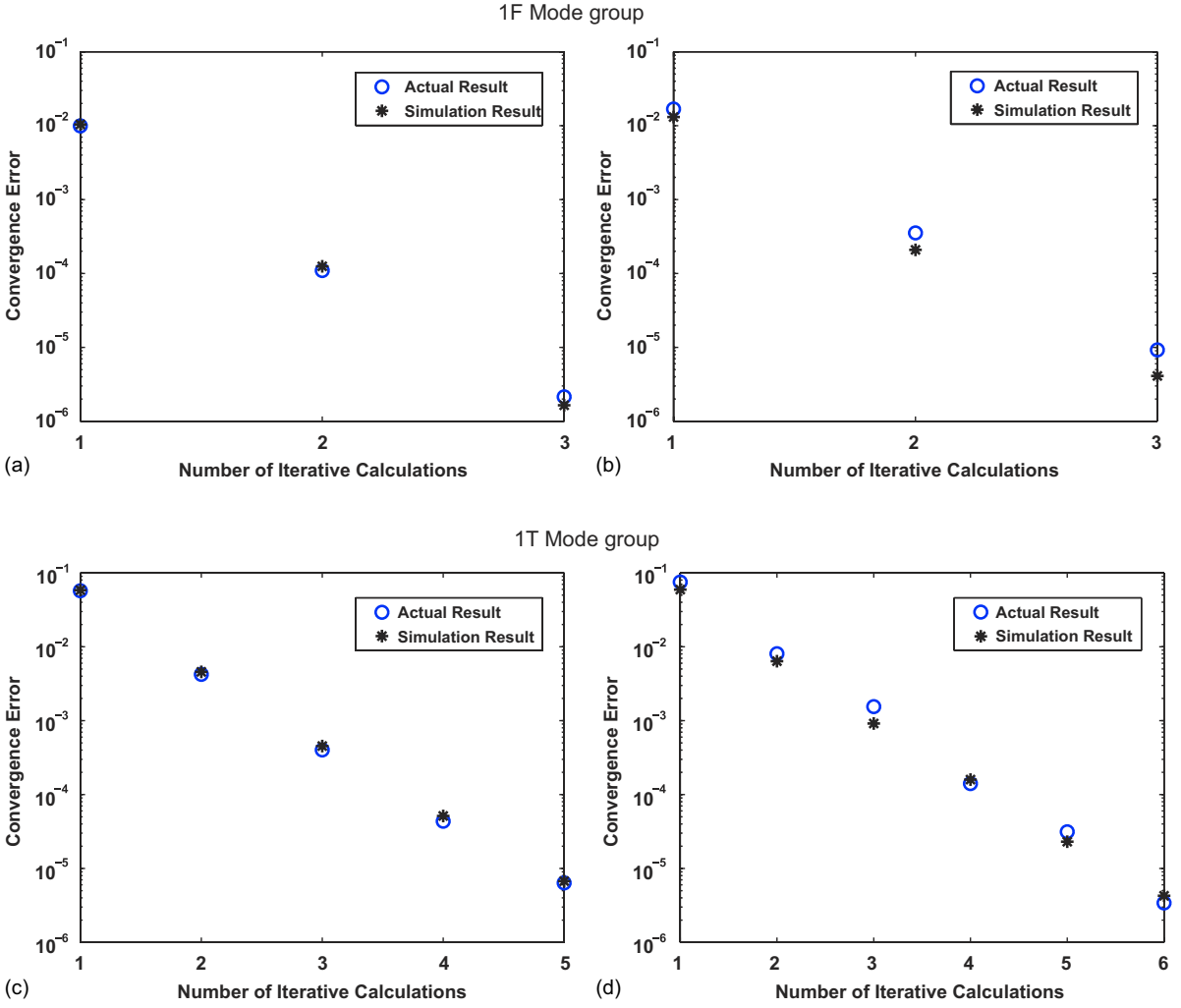


Fig. 3. Convergence errors of the actual calculation and the hybrid technique using the actual matrices: (a) and (c) tuned cases; (b) and (d) mistuned cases.

convergence errors are closer to the broader ranges of the Monte Carlo predictions (i.e. Fig. 4). Also, the first-step results in Figs. 4 and 5 are less accurate than the results after more iterations. For the results after more iterations, the changes in the complex frequencies (compared with results of the last iterative step) become smaller. Therefore, the assumption of linearity between aerodynamic forces and complex frequencies is more closely satisfied, and the hybrid approach is more accurate.

Table 2 shows the relative errors of the converged results using the hybrid method compared with the actual converged results. For the 1F frequency range, the errors are small (although above $10^{-5}$). For the 1T frequency range, the errors are larger. This is likely caused by the fact that, having a veering region, the eigenvalues in the 1T frequency range have a broader range than those in the 1F frequency range. Hence, the errors become larger. However, the purpose of the hybrid technique is to predict the *convergence history* of the aeroelastic calculation correctly and quickly, and not to predict the actual aeroelastic results.

### 5.2. General Monte Carlo simulation

To investigate the effects of various factors on the iteration convergence, a Monte Carlo simulation is performed by changing two ratios while other ratios are kept constant. For every combination of these ratios, all the matrices are

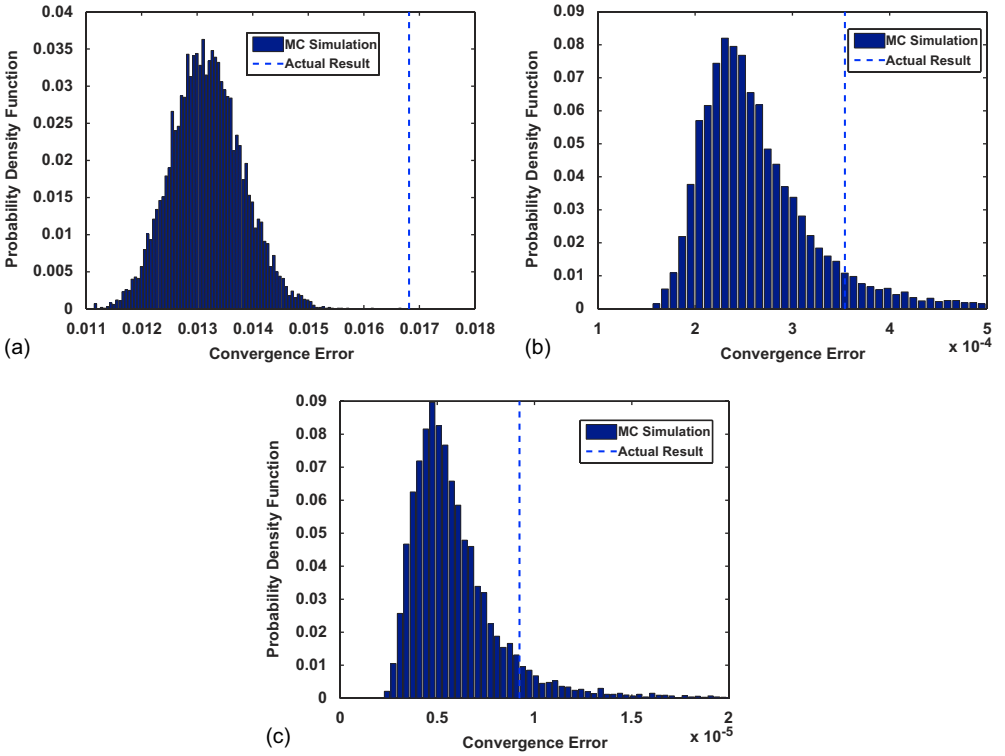


Fig. 4. Probability density function of results using the perturbed matrices for the mistuned case in the 1F frequency range: (a) first step; (b) second step; and (c) third step.

determined randomly by matching the ratios and the predefined reference frequency. Actually, under this formulation, the results will hold irrespective of the reference frequency. The dimension of the system is 10 for normal cases and 12 for cases with a frequency veering region. Usually, actual systems have larger dimensions. However, a 10-dimension system is considered large enough to study the effects of critical factors. Ten thousand samples are used for every combination of the ratios. The nominal values of the ratios are 0.3 for $r_A$, 1.0 for $r_G$, 0.01 for $r_F$, 0 for $r_V$, 0.2 for $r_M$, and 0.001 for $\gamma$.

Fig. 6 shows the convergence error with changing $r_A$ and $r_G$. The mean error, as well as the 90% confidence levels are plotted. As shown in Fig. 7, for a confidence $1-\alpha$, a $\alpha/2$ portion of all the samples fall below the lower confidence level $\delta_l$ and fall beyond the upper confidence level $\delta_u$ (Bury, 1975). Also shown in Fig. 7 is the average (mean) error $\delta_a$. When $r_A = 0$ or $r_G = 0$, which represents no aerodynamic influence or no aerodynamic matrix dependence on the complex frequency, the convergence error is zero. The convergence error becomes larger when $r_A$ or $r_G$ grows. If both $r_A$ and $r_G$ are very large, convergence cannot be achieved. This phenomenon is not shown in Fig. 6 because the iterative calculation fails in such a situation. A large $r_A$ indicates that the system has a large aerodynamic matrix, which can change the complex aeroelastic frequency significantly. A large $r_G$ makes this aerodynamic matrix sensitive to the change of aeroelastic natural frequencies. Hence, the iterative process fails to converge when $r_A$ and $r_G$ are both large. Note that the computation time for one iteration step in this case is about 70 min with 10 000 samples.

Fig. 8 shows the convergence error with changing $r_F$ and $r_V$. The basic trend is that the system converges slower when $r_F$ or $r_V$ becomes smaller. However, the effect is relatively small, and there is no case in which convergence cannot be achieved.

The convergence error with changing $r_M$ and $\gamma$ is shown in Fig. 9. The structural damping $\gamma$ has no significant effect on the convergence error. When the mistuning ratio $r_M$ becomes larger, the convergence error first grows rapidly, then drops, and finally approaches a constant value. The mistuned system converges always slower than the tuned one. There are two major consequences of the growth of $r_M$. First, the differences between the tuned and mistuned structural frequencies become larger. Second, the off-diagonal terms in $\mathbf{Q}_{\phi}^{S,n}$ become larger. Note that when the system is tuned,

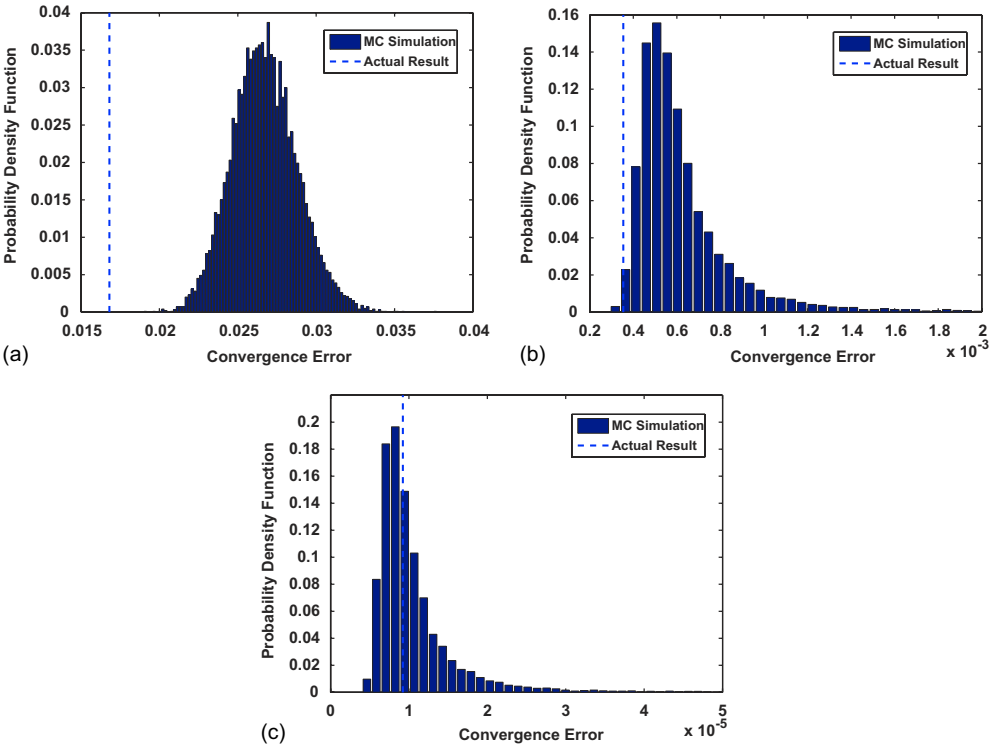


Fig. 5. Probability density function of results using the totally random matrices for the mistuned case in the 1F frequency range: (a) first step; (b) second step; and (c) third step.

Table 2
Relative errors between simulated converged results and actual converged results

| System | 1F tuned | 1F mistuned | 1T tuned | 1T mistuned |
|---|---|---|---|---|
| Error | $8.35 \times 10^{-5}$ | $6.55 \times 10^{-4}$ | $4.36 \times 10^{-3}$ | $1.77 \times 10^{-2}$ |

$\mathbf{Q}_{\phi}^{S,n}$ is a block diagonal matrix. Both factors make the matrices $\mathbf{T}^R$ and $\mathbf{T}^I$ in Eq. (21) have larger variations during the iterations. When the mistuning level is relatively small, this effect dominates, and the system converges harder. However, when the mistuning level is very large, the combined (tuned and mistuned) structural stiffness matrix becomes larger, which makes the relative effect of the aerodynamic matrix smaller. Then, the system exhibits a slow reduction in the convergence error. Also, overall, the effect of $r_M$ on the convergence is small compared to $r_A$ and $r_G$.

As shown in Fig. 3, the convergence error is larger for a mistuned system than a tuned system, which can be predicted from Fig. 9. Also, the convergence error is larger for the 1T frequency range than for the 1F frequency range. From Table 1, the major differences between the critical ratios for these two frequency ranges are $r_G$ and $r_V$. Because the effect of $r_V$ is not very significant, the larger value of $r_G$ for the 1T range is the major reason for the slower convergence in this frequency range.

Fig. 10 shows the convergence error with changing $r_A$ and $\gamma$. The structural damping has no significant effect on the convergence error. The convergence error increases quickly when the aero ratio $r_A$ becomes larger. Fig. 11 shows the convergence error for various ratios $r_F$ and $r_M$. The effect of the frequency ratio $r_F$ on the convergence error is small. When the mistuning ratio $r_M$ increases (from 0), the convergence error increases rapidly first, and then decreases smoothly. Fig. 12 shows the convergence error for various $r_G$ and $r_V$. A larger gradient ratio $r_G$ makes the aeroelastic iterations harder to converge, while a larger veering ratio $r_V$ makes the iterations easier to converge. However, the effect of $r_G$ is much more significant than $r_V$.

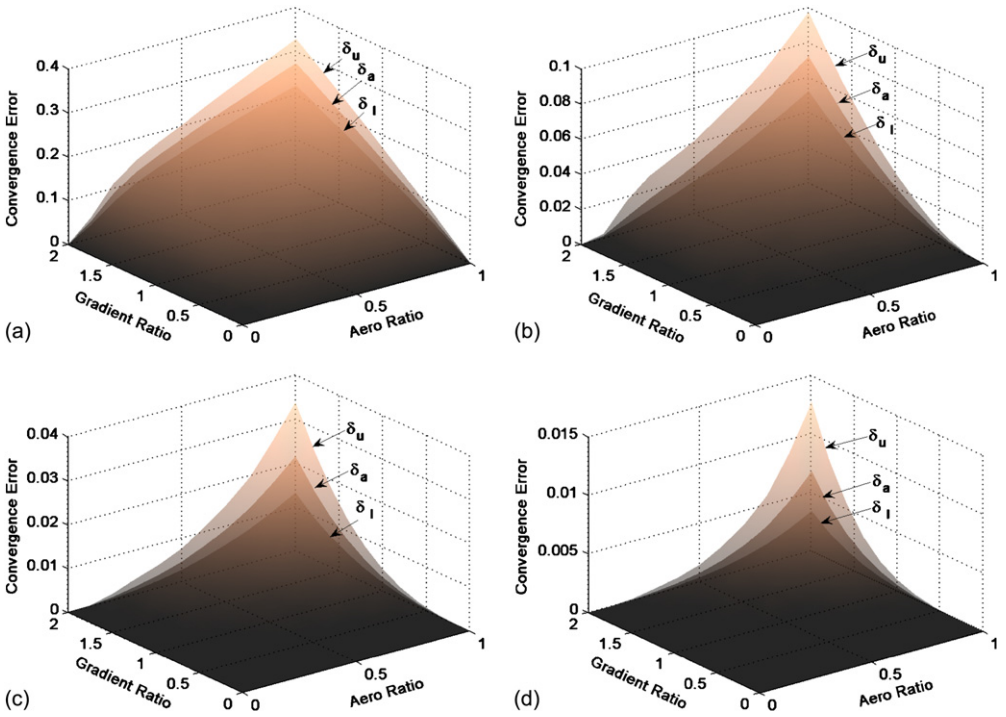


Fig. 6. Monte Carlo simulation results (mean error $\delta_a$ and error limits $\delta_u$ and $\delta_l$ of 90% confidence level) for a mistuned system with changing $r_A$ and $r_G$. (a) First step; (b) second step; (c) third step; (d) fourth step.

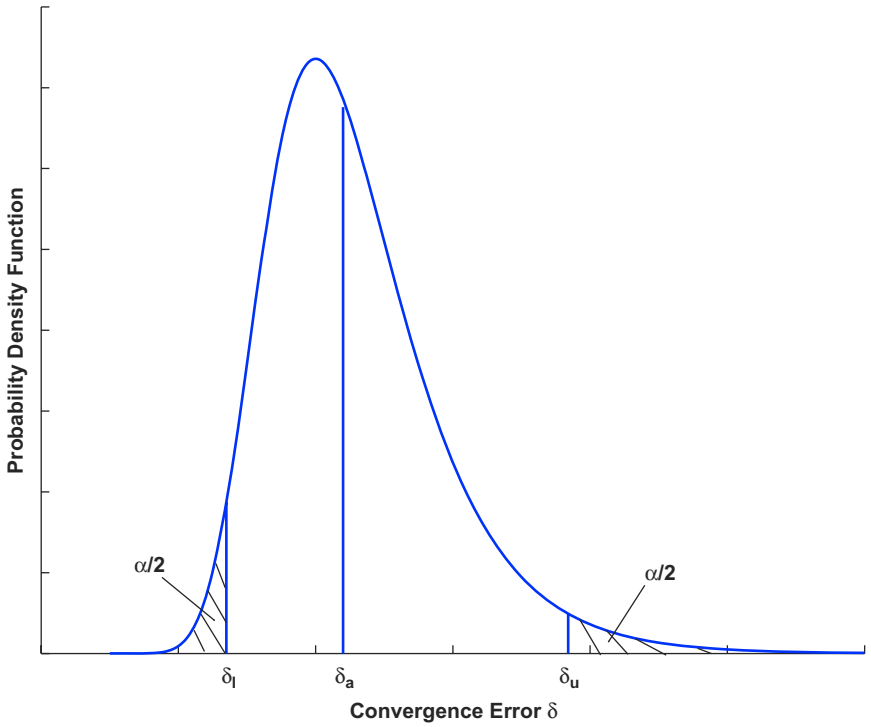


Fig. 7. Illustration of confidence levels with confidence $1-\alpha$.

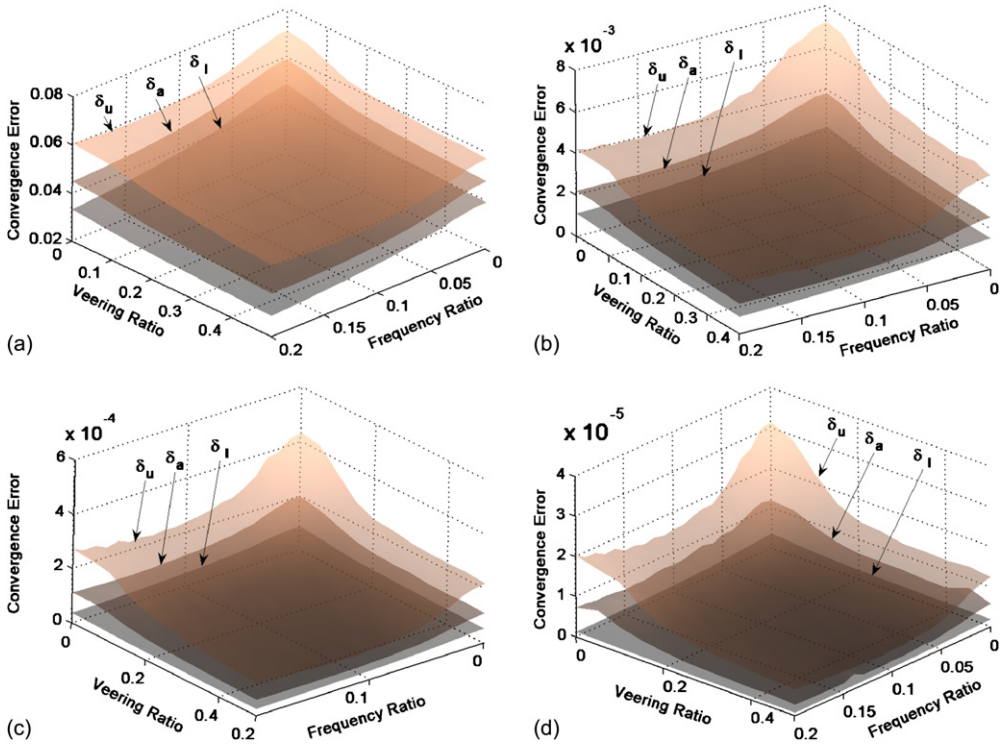


Fig. 8. Monte Carlo simulation results (mean error $\delta_a$ and error limits $\delta_u$ and $\delta_l$ of 90% confidence level) for a mistuned system with changing $r_F$ and $r_V$. (a) First step; (b) second step; (c) third step; (d) fourth step.

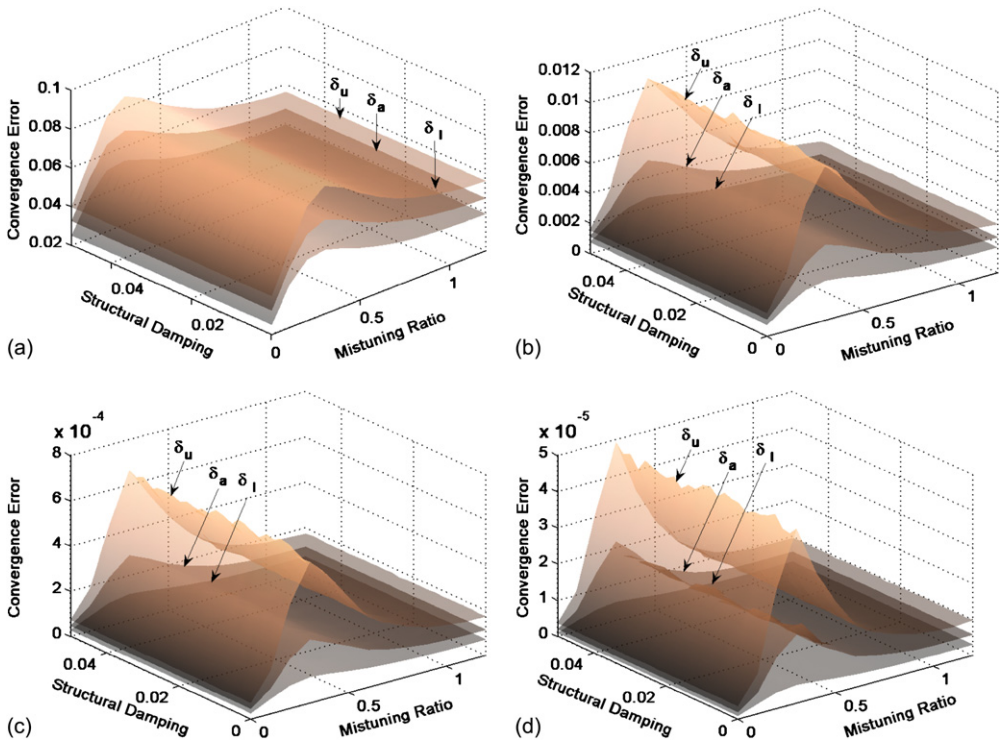


Fig. 9. Monte Carlo simulation results (mean error $\delta_a$ and error limits $\delta_u$ and $\delta_l$ of 90% confidence level) for a mistuned system with changing $r_M$ and $\gamma$. (a) First step; (b) second step; (c) third step; (d) fourth step.

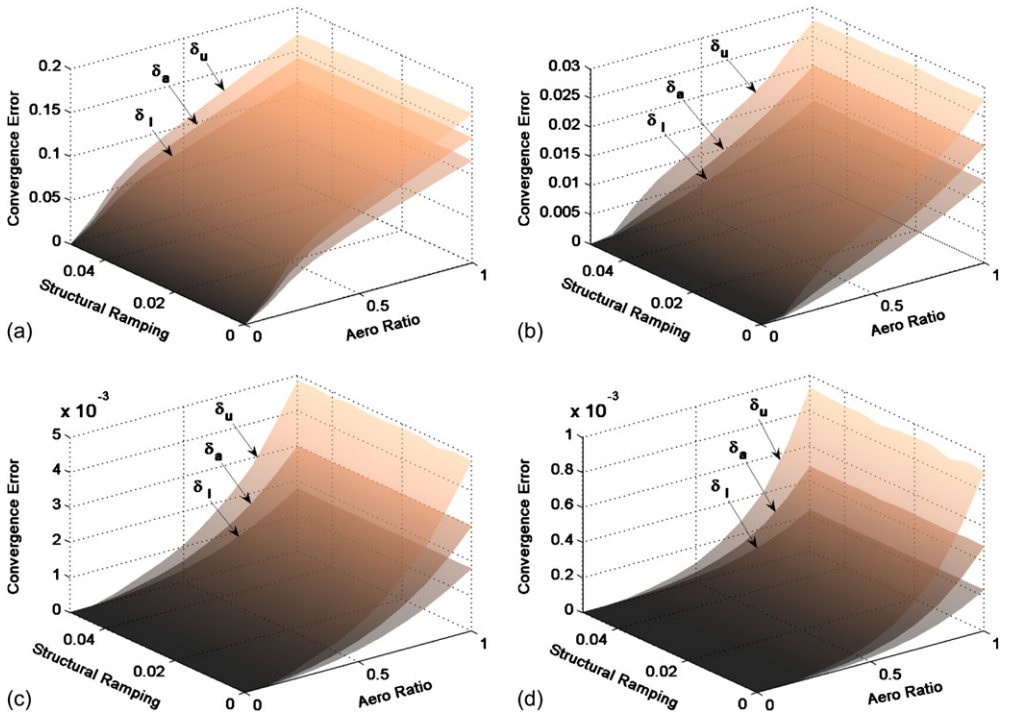


Fig. 10. Monte Carlo simulation results (mean error $\delta_a$ and error limits $\delta_u$ and $\delta_l$ of 90% confidence level) for a mistuned system with changing $r_A$ and $\gamma$. (a) First step; (b) second step; (c) third step; (d) fourth step.

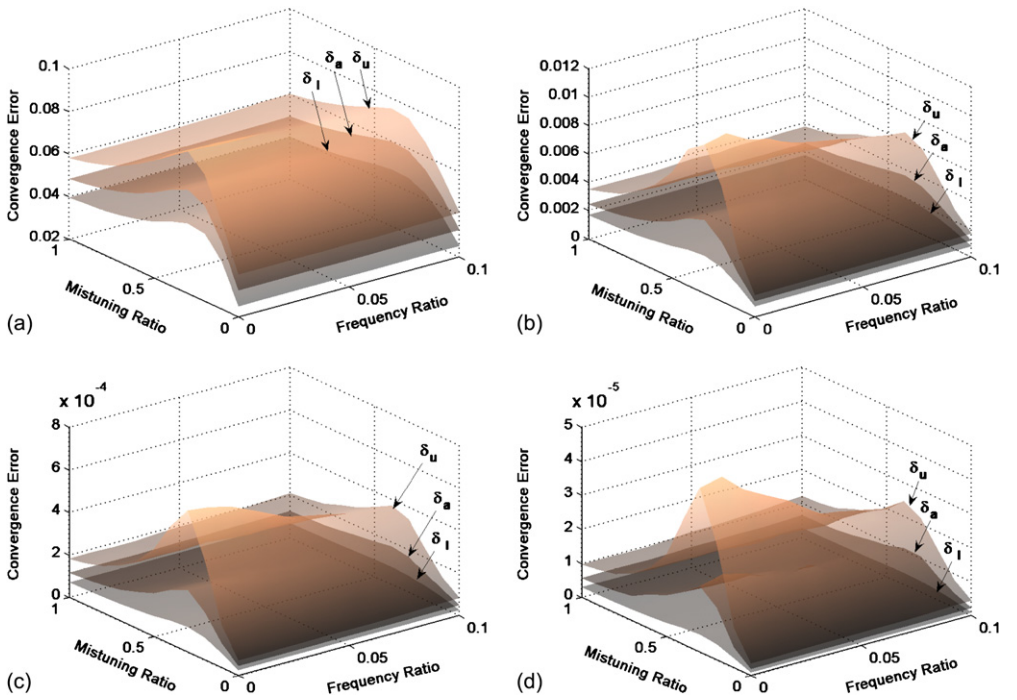


Fig. 11. Monte Carlo simulation results (mean error $\delta_a$ and error limits $\delta_u$ and $\delta_l$ of 90% confidence level) for a mistuned system with changing $r_F$ and $r_M$. (a) First step; (b) second step; (c) third step; (d) fourth step.

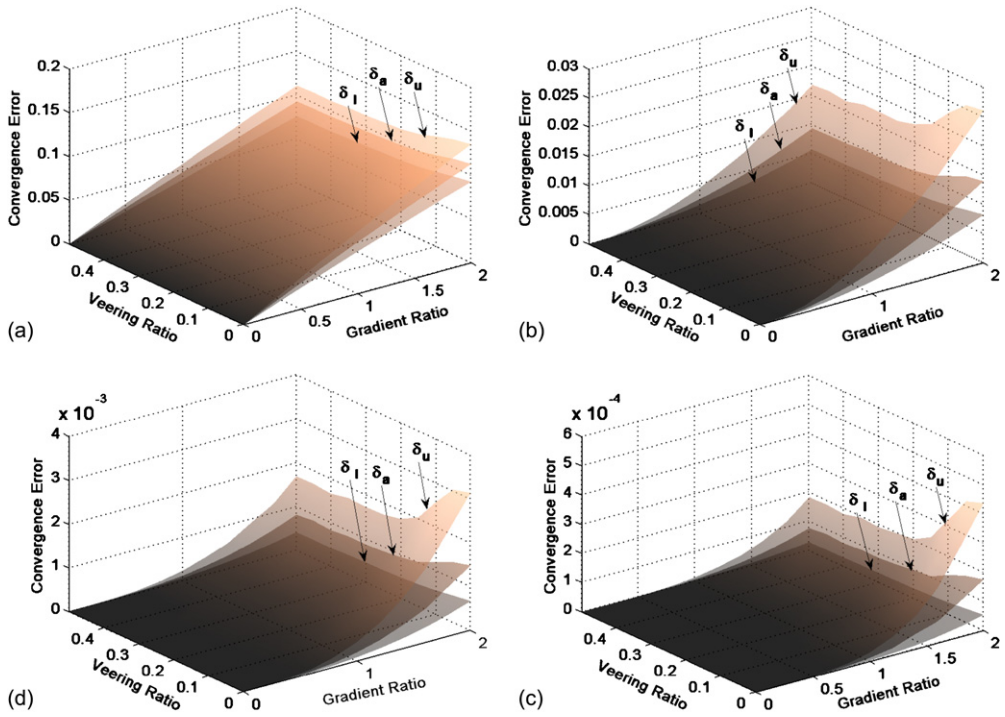


Fig. 12. Monte Carlo simulation results (mean error $\delta_a$ and error limits $\delta_u$ and $\delta_l$ of 90% confidence level) for a mistuned system with changing $r_G$ and $r_V$. (a) First step; (b) second step; (c) third step; (d) fourth step.

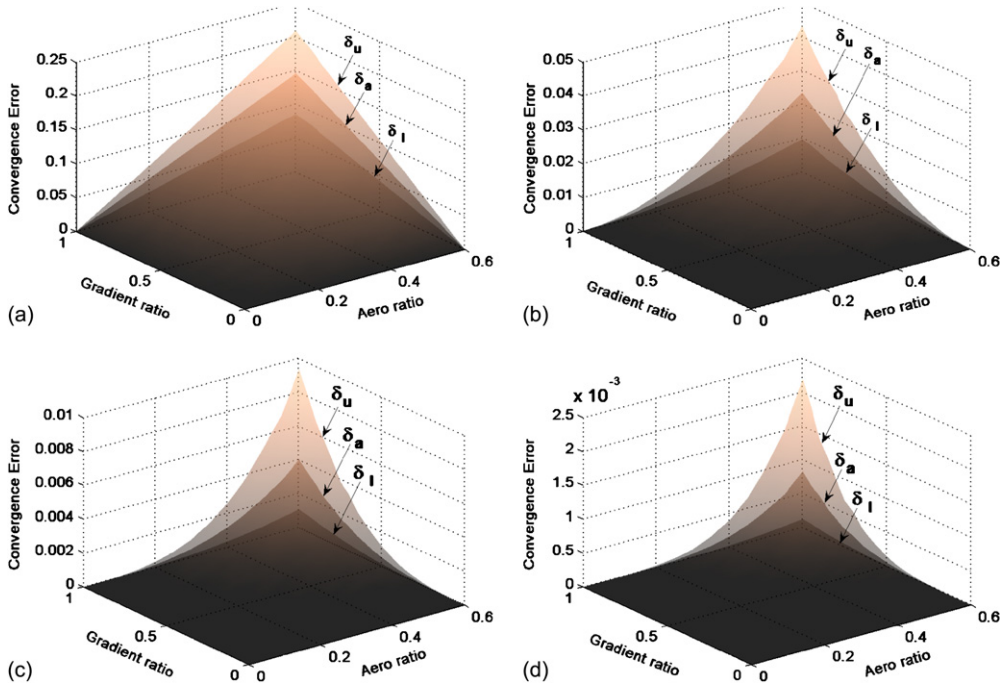


Fig. 13. Monte Carlo simulation results (mean error $\delta_a$ and error limits $\delta_u$ and $\delta_l$ of 90% confidence level) for a tuned system with changing $r_A^T$ and $r_G^T$. (a) First step; (b) second step; (c) third step; (d) fourth step.

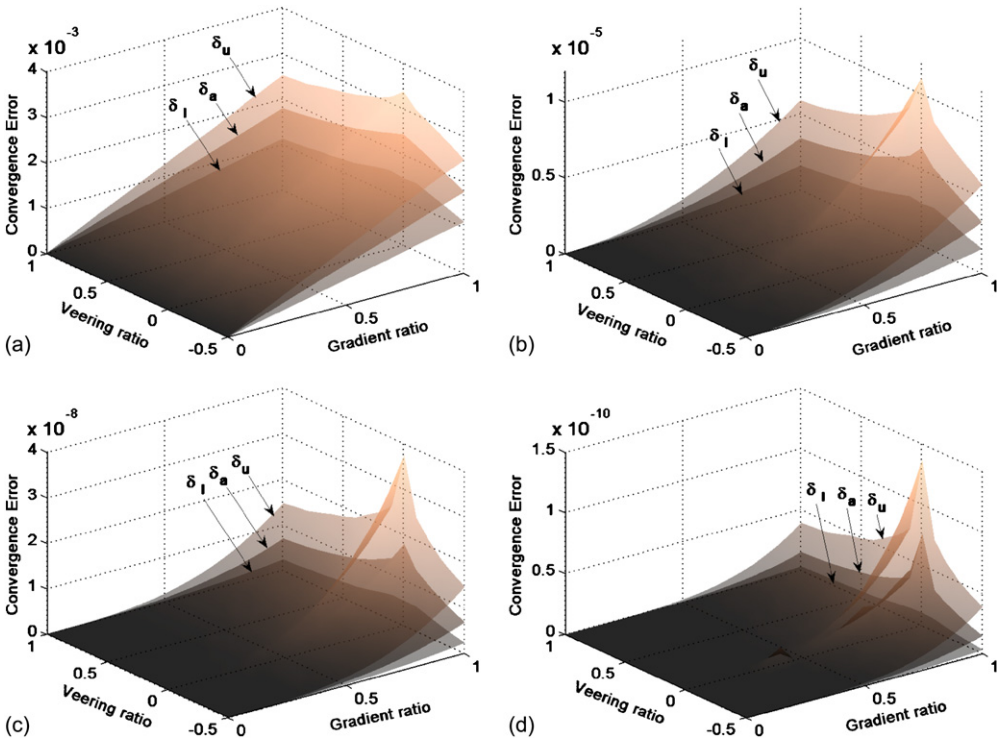


Fig. 14. Monte Carlo simulation results (mean error $\delta_a$ and error limits $\delta_u$ and $\delta_l$ of 90% confidence level) for a tuned system with changing $r_G^T$ and $r_V^T$. (a) First step; (b) second step; (c) third step; (d) fourth step.

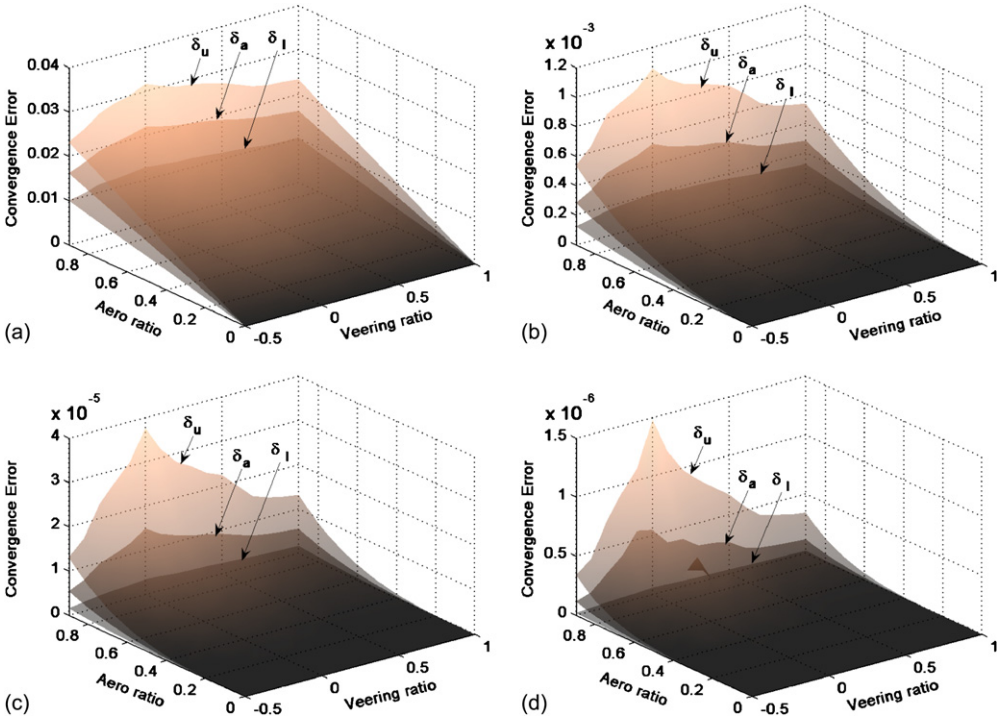


Fig. 15. Monte Carlo simulation results (mean error $\delta_a$ and error limits $\delta_u$ and $\delta_l$ of 90% confidence level) for a tuned system with changing $r_V^T$ and $r_A^T$. (a) First step; (b) second step; (c) third step; (d) fourth step.

### 5.3. Monte Carlo simulation: tuned system

A tuned system described in Section 4 is studied. The only critical ratios considered here are $r_A^T$, $r_G^T$, and $r_V^T$. Ten thousand samples for every combination of these ratios are used for the Monte Carlo simulation. The smallest one of the tuned undamped structural natural frequencies is used as a reference frequency. For this case, the largest relative error in the aerodynamic damping with one-step calculation is 20% compared to the converged result.

Fig. 13 shows the convergence error with changing $r_A^T$ and $r_G^T$. The veering ratio $r_V^T$ is 0. Similar to Fig. 6, larger $r_A^T$ and $r_G^T$ make the aeroelastic calculation harder to converge. This is consistent with Moyroud et al. (1996), where Moyroud et al. state that tuned bladed disks made of composites are harder to converge than the tuned bladed disks made of metallic alloys. This is explained herein by the fact that, for composite bladed disks, the ratios $r_A^T$ and $r_G^T$ are smaller than those of metallic bladed disks under the same operation point and with the same geometry. Actually, from Section 5.2, this conclusion also holds for the mistuned case. The convergence error with changing $r_G^T$ and $r_V^T$ is shown in Fig. 14. The aero ratio $r_A^T$ is 0.01. Similar to Fig. 8, when the frequencies $\omega_{01}$ and $\omega_{02}$ (in Eq. (30)) are closer, the aeroelastic calculation becomes harder to converge. This result is particularly useful to be compared with the discussions of Gerolymos (1993) who states that for a tuned system, the stability of the iterations requires that the eigenfrequencies are well separated. Note that in Fig. 13, a system with a zero value of $r_V^T$ can converge fast if both $r_A^T$ and $r_G^T$ are small. Also, note that Figs. 8 and 14 show a relatively small effect of $r_V^T$ on the convergence error. This seems somewhat contrary to Gerolymos' (1993) results. However, in Gerolymos (1993), the iteration is formulated using a mode-modification technique, which calculates the tuned aeroelastic eigenvalues and eigenvectors separately for every aeroelastic mode. The aeroelastic calculations shown in Sections 3 and 4 are formulated by solving the aeroelastic eigenvalue problem directly. Although this method requires more computation time for finding eigenvalues and eigenvectors, it is shown that it is better than the mode-modification technique in the sense of convergence. Fig. 15 shows the convergence error for various $r_V^T$ and $r_A^T$. The convergence error increases quickly with increasing $r_A^T$, and the aeroelastic iterations become harder to converge when $r_V^T$ approaches 0.

## 6. Conclusions

A hybrid technique has been proposed to predict the convergence error of the aeroelastic calculation for mistuned bladed disks. The dependence of the aerodynamic forces on vibration frequencies has been approximated linearly by proposing an aero ratio based on two aerodynamic gradient matrices. Several other critical ratios have been defined to study their effects on the convergence error. Matrices randomly generated according to these critical ratios, as well as the exact matrices of an actual model, can be used in this hybrid technique. The hybrid technique has been validated using the exact matrices calculated for an actual industrial bladed disk. Monte Carlo simulations for general mistuned systems and tuned systems have been performed, and several conclusions have been obtained for the bladed disk studied.

First, the aero ratio $r_A$ and the gradient ratio $r_G$ have significant effects on the convergence error. For a system with both large $r_A$ and $r_G$, an iterative calculation is likely to be unable to converge.

Second, the mistuned aeroelastic calculation is harder to converge than the corresponding tuned calculation. When the mistuning level is small, increases in the mistuning ratio $r_M$ make the system harder to converge. While the mistuning level is large, the convergence error decreases slowly when $r_M$ grows. In general, $r_M$ has a moderate effect on the convergence error.

Third, a smaller veering ratio $r_V$ or a smaller frequency ratio $r_F$ makes the system harder to converge. However, the effect is relatively small. Finally, the structural damping $\gamma$ has no significant effect on the convergence error.

## Acknowledgments

The authors gratefully acknowledge the support of the GUIde Consortium on Blade Durability at Carnegie Mellon University and the Air Force Office of Scientific Research.

## References

Anderson, P.W., 1958. Absence of diffusion in certain random lattices. Physical Review 109 (5), 1492–1505.

Bell, D.L., He, L., 2000. Three-dimensional unsteady flow for an oscillating turbine blade and the influence of tip leakage. ASME Journal of Turbomachinery 122 (1), 93–101.

Bladh, J.R., 2001. Efficient predictions of the vibratory response of mistuned bladed disks by reduced order modeling. Ph.D. Thesis, The University of Michigan, Ann Arbor, MI.

Bladh, R., Castanier, M.P., Pierre, C., 2001a. Component-mode-based reduced order modeling techniques for mistuned bladed disks, Part I: theoretical models. ASME Journal of Engineering for Gas Turbines and Power 123 (1), 89–99.

Bladh, R., Castanier, M.P., Pierre, C., 2001b. Component-mode-based reduced order modeling techniques for mistuned bladed disks, Part II: application. ASME Journal of Engineering for Gas Turbines and Power 123 (1), 100–108.

Bury, K.V., 1975. Statistical Models in Applied Science. Wiley, New York, NY, pp. 118–121.

Chaviaropoulos, P.K., Hansen, M.O.L., 2000. Investigating three-dimensional and rotational effects on wind turbine blades by means of a quasi-3D Navier–Stokes solver. ASME Journal of Fluids Engineering 122 (2), 330–336.

Crawley, E.F., Hall, K.C., 1985. Optimization and mechanisms of mistuning in cascades. ASME Journal of Engineering for Gas Turbines and Power 107 (2), 418–426.

Feiner, D.M., Griffin, G.H., 2002. A fundamental model of mistuning for a single family of modes. ASME Journal of Turbomachinery 124 (4), 597–605.

Fransson, T.H., Jöcker, M., Bölcs, A., Ott, P., 1999. Viscous and inviscid linear/nonlinear calculations versus quasi-three-dimensional experimental cascade data for a new aeroelastic turbine standard configuration. ASME Journal of Turbomachinery 121 (4), 717–725.

Gerolymos, G.A., 1993. Coupled three-dimensional aeroelastic stability analysis of bladed disks. ASME Journal of Turbomachinery 115 (4), 791–799.

Hall, K.C., 1993. Deforming grid variational principle for unsteady small disturbance flows in cascades. AIAA Journal 31 (5), 891–900.

Hall, K.C., Lorence, C.B., 1993. Calculation of three-dimensional unsteady flows in turbomachinery using the linearized harmonic Euler equations. ASME Journal of Turbomachinery 115 (4), 800–809.

Hall, K.C., Lorence, B.C., Clark, W.S., 1993. Nonreflecting boundary conditions for linearized unsteady aerodynamic calculations. In: AIAA Paper 1993-882, Proceedings of the 31st Aerospace Sciences Meeting and Exhibit, Reno, NV, USA.

He, Z., Epureanu, B.I., Pierre, C., 2005a. Effects of unsteady aerodynamics on the dynamic response of mistuned bladed disks. In: Proceedings of the 3rd MIT Conference on Computational Fluid and Solid Mechanics, Boston, MA, USA.

He, Z., Epureanu, B.I., Pierre, C., 2005b. Influence of aerodynamic coupling on the dynamics of mistuned bladed disks. In: Proceedings of the 10th National Turbine Engine High Cycle Fatigue Conference, New Orleans, LA, USA.

He, Z., Epureanu, B.I., Pierre, C., 2006. A novel hybrid method to predict the convergence history of aeroelastic calculations of mistuned/tuned bladed disks. In: Proceedings of the ASME Pressure Vessels and Piping Conference 2006, vol. 9, pp. 719–729.

Kaza, K.R.V., Kielb, R.E., 1984. Flutter of turbofan rotors with mistuned blades. AIAA Journal 22 (11), 1618–1625.

Kaza, K.R.V., Kielb, R.E., 1985. Vibration and flutter of mistuned bladed-disk assemblies. AIAA Journal of Propulsion and Power 1 (5), 336–344.

Khader, N., Loewy, R., 1989. Shaft flexibility effects on aeroelastic stability of a rotating bladed disk. AIAA Journal of Propulsion and Power 5 (6), 718–726.

Kielb, R.E., Feiner, D.M., Griffin, J.H., Miyakozawa, T., 2004a. Flutter of mistuned bladed disks and blisks with aerodynamic and fmm structural coupling. In: Proceedings of ASME Turbo Expo 2004, vol. 6, pp. 573–579.

Kielb, R.E., Feiner, D.M., Griffin, J.H., Miyakozawa, T., 2004b. Probabilistic analysis of mistuned bladed disks and blisks with aerodynamic and fmm structural coupling. In: Proceedings of the 9th National Turbine Engine HCF Conference.

Lim, S., Bladh, R., Castanier, M.P., Pierre, C., 2003. A compact, generalized component mode mistuning representation for modeling bladed disk vibrations. In: AIAA Paper 2003-1545, Proceedings of the 44th AIAA/ASME/ASCE/AMS Structures, Structural Dynamics and Material Conference, Norfolk, VA, USA.

Moyroud, F., Jacquet-Richardet, G., Fransson, T., 1996. A modal coupling for fluid and structure analyses of turbomachine flutter. Application to a fan stage. In: ASME Paper 96-GT-335, Proceedings of ASME Turbo Expo 1996.

Petrov, E.P., Sanliturk, K.Y., Ewins, D.J., 2002. A new method for dynamic analysis of mistuned bladed disks based on the exact relationship between tuned and mistuned systems. ASME Journal of Engineering for Gas Turbines and Power 124 (3), 586–597.

Seinturier, E., Dupont, C., Berthillier, M., Dumas, M., 2002. A new aeroelastic model for mistuned bladed disks. In: AIAA Paper 2002-1533, Proceedings of the 43rd AIAA/ASME/ASCE/AHS/ASC Structures, Structural Dynamics, and Materials Conference.

Tobias, S.A., Arnold, R.N., 1957. The influence of dynamical imperfection on the vibration of rotating disks. Proceedings of the Institution of Mechanical Engineers 171, 669–690.

Wei, S.T., Pierre, C., 1988a. Localization phenomena in mistuned assemblies with cyclic symmetry. Part I: free vibrations. ASME Journal of Vibration, Acoustics, Stress and Reliability in Design 110 (4), 429–438.

Wei, S.T., Pierre, C., 1988b. Localization phenomena in mistuned assemblies with cyclic symmetry. Part II: forced vibrations. ASME Journal of Vibration, Acoustics, Stress and Reliability in Design 110 (4), 439–449.

Yang, M.T., Griffin, J.H., 2001a. A normalized modal eigenvalue approach for resolving modal interaction. ASME Journal of Engineering for Gas Turbines and Power 119 (3), 647–650.

Yang, M.T., Griffin, J.H., 2001b. A reduced-order model of mistuning using a subset of nominal system modes. ASME Journal of Engineering for Gas Turbines and Power 123 (4), 893–900.